Taylor & Francis
Taylor & Francis Group

Advanced Composite Materials

ISSN: 0924-3046 (Print) 1568-5519 (Online) Journal homepage: http://www.tandfonline.com/loi/tacm20

Performance index optimization of pressure vessels manufactured by filament winding technology

L. Sorrentino & L. Tersigni

To cite this article: L. Sorrentino & L. Tersigni (2015) Performance index optimization of pressure vessels manufactured by filament winding technology, Advanced Composite Materials, 24:3, 269-285, DOI: 10.1080/09243046.2014.887429

To link to this article: http://dx.doi.org/10.1080/09243046.2014.887429

Advanced Composite Materials, 2015
Vol. 24, No. 3, 269–285, http://dx.doi.org/10.1080/09243046.2014.887429

Performance index optimization of pressure vessels manufactured by filament winding technology

L. Sorrentino* and L. Tersigni

Department of Civil and Mechanical Engineering, University of Cassino and Southern Lazio, Cassino 03043, Italy

(*Received 27 March 2013; accepted 22 January 2014*)

Filament-wound pressure vessels represent the proper choice to obtain good mechanical properties and lightweight. The pressure vessel geometry is generally cylindrical and the wall is composed of a 'liner' and a 'shell.' The liner holds the gas and guards the shell from chemical attacks. The filament-wound shell aims to withstand the hydrostatic load of pressure gas. The shell design has to be defined in observance of both fibers stratification methodology and design structural criteria. For years, pressure vessel design primarily focused on mass; space saving features during pressure vessel design was usually a secondary concern unless specifically required by the customer. Now, more emphasis have being assigned to design light weight pressure vessels that also maximizes use of available space for industry finding such as space on a spacecraft, as well as mass, is at premium. For this reason, it is very important to optimize together the index of performance and packaging of gas storage system. This work aims to develop a parametric method to optimize the index of performance as a function of one or more pressure vessels; in this way, it is possible to optimize also the packaging of the gas storage system.

keywords: composite material; pressure vessel; filament winding; performance index; packaging

1. Introduction

The fibers reinforced plastic is used more and more for the manufacturing of components that need high mechanical performances and lightweight. An example is given by the composite pressure vessels for gas storage which are much lighter than comparable all-metal pressure vessels for development of unmanned aerial vehicle (UAV). UAV is a solar-powered, ultra lightweight, high-altitude, long duration flying wing. During the day, the aircraft is powered by solar energy, and at night it is to be powered by a unique fuel cell system. This system requires lightweight pressure vessels containing both the hydrogen and oxygen constituents of the fuel cell. Another potential widespread application for composite pressure vessels is the automotive industry where the need to reduce emissions promotes the conversion to compressed natural gas fuelled vehicles worldwide; natural gas or hydrogen as the energy supply in automobiles for air quality improvements and reduce global warning.[1,2] Although composite pressure vessels appear to be simple structures, they are among the most difficult to design and manufacture. Filament-wound pressure vessels represent the proper choice to obtain

*Corresponding author. Email: sorrentino@unicas.it

good mechanical properties and lightweight.[3–22] The pressure vessel geometry is generally cylindrical and the wall is composed of a 'liner' and a 'shell.' The liner holds the gas and guards the shell from chemical attacks. The filament-wound shell aims to withstand the hydrostatic load of pressure gas. The shell design has to be defined in observance of both fibers stratification methodology and design structural criteria. For years, pressure vessel design primarily focused on mass. Space saving features during pressure vessel design has been usually a secondary concern unless specifically required by the customer. Now more emphasis has been assigned to design lightweight pressure vessels that also maximizes use of available space for industry finding such as space on a spacecraft, as well as mass, is at premium. A very important parameter characterizing performance and lightweight of pressure vessels is the Index-of-Performance calculated as $I_p = p \cdot v/(m \cdot g)$ (m), where the p, v, m, and g are, respectively, the pressure, the volume, the mass, and the acceleration of gravity. Higher the I_p, more performing is the pressure vessel.[23–26] For this reason, it is very important to optimize together the index of performance and packaging of gas storage system. This work aims to develop a parametric method to optimize the index of performance as a function of one or more pressure vessels; in this way it is possible to optimize also the packaging of the gas storage system.

2. Design of filament-wound pressure vessel

In this work, a pressurized tank has been considered. It is made of a cylindrical section, height h, and two caps on endings, the internal volume is called v; the geometry is shown in Figure 1. The structural part (shell) is constituted in composite material, the inner surface of all laminates consist of a protective layer. The protective layer can be either a single protective layer or a chemical resistant layer or a thermoplastic lining. The type of protective layer can be selected on the basis of the ability to prevent, or

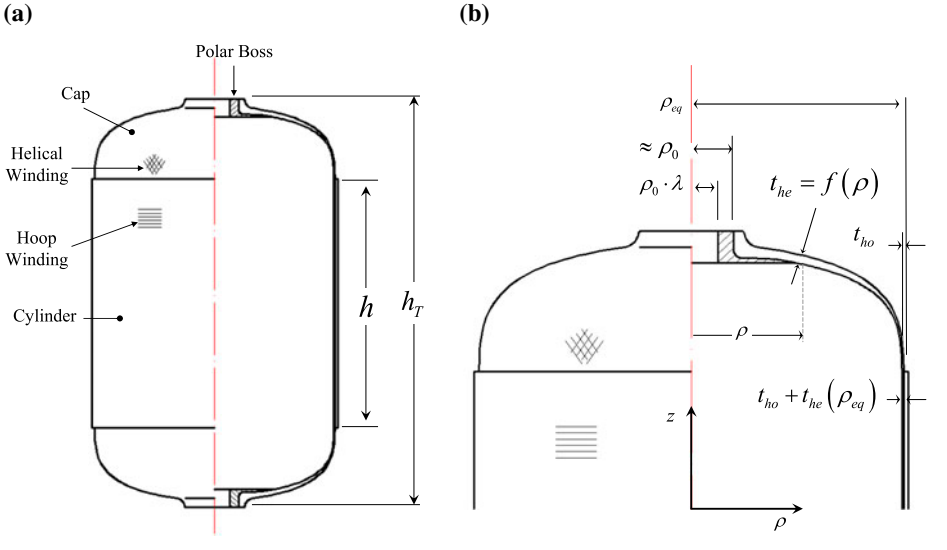

Figure 1. (a) Filament-wound pressure vessel; (b) Cross-section of pressure vessel.

limit to an acceptable level, chemical attack on the laminate. In order to do this, it can be chemically resistant to the service conditions, allow limited diffusion of service fluids and shall not suffer environmental stress cracking. The liner may be applied to the mandrel prior to the start of the winding operation; in this paper, a polymeric liner with constant thickness has been considered. The shell is constituted by two kinds of windings: 'helical winding' and 'hoop winding' shown in Figure 1. The helical winding involves both the cylindrical and cap area while the hoop winding involve the cylindrical area only. At the end of the tank, a polar boss helps the structural strength in that area and allows the connection with the system.

The pressure vessels are manufactured by winding of a tape impregnated by resin on a mandrel with sufficient rigidity and dimensional stability to resist the winding load and the compressive loads which occur during the cure cycle. In this work, a vessel design has been carried out starting from the caps features (helical winding) and then to the cylindrical area (helical and hoop winding).

2.1. *Caps: outline meridian definition*

The caps geometry has been defined through the meridian outline that has to be correctly calculated as function of stress caused by vessel internal pressure. Generally, stress on caps caused by pressure (p) is bore by helical winding only (Figure 2) for which an isotensoidal condition has been considered (for every single tow a constant force F has been considered). The contribution of these windings in the axial direction (axe z) can be described by the following equation:

$$A_f = F \cdot n_{he} \cos\alpha \cos\beta \tag{1}$$

were A_f is total axial force while n_{he} is the number of tows wound with a helical winding and $F\cos\alpha{\cdot}\cos\beta$ is the force that supports a single tow (see Figure 3). Carrying out the axial balance with the internal pressure force p, we have:

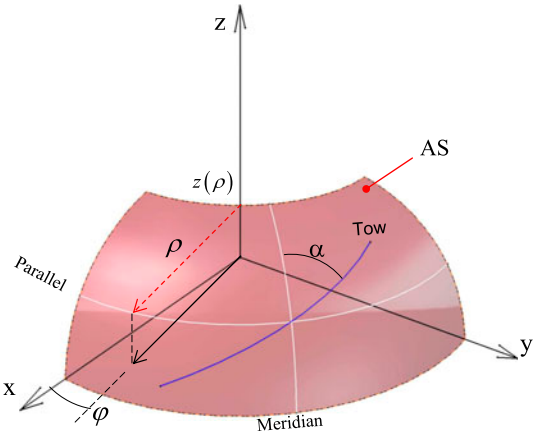

Figure 2. Axial symmetric surface described by polar coordinates, with: α, tow angle respect to the meridian; δ, angle between meridian and parallel; φ and ρ, polar system coordinates (angle and distance).

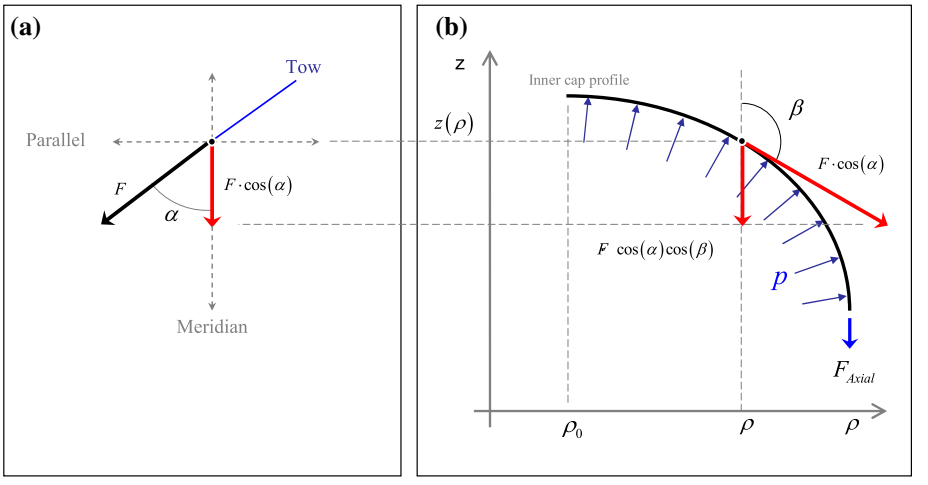

Figure 3. Forces induced by tow in axial direction in a cap point (views of a plan that is tangent to the meridian): (a) plan frontal view; (b) plan lateral view.

$$-F \cdot n_{he} \cos\alpha \cos\beta = p\pi\rho^2 \times 10^{-6} \tag{2}$$

From which, substituting the following equation:

$$\cos\beta = \frac{Z'(Y)}{\sqrt{1+Z'(Y)^2}}, \quad Z = \frac{z}{\rho_0}, \quad Y = \frac{\rho}{\rho_0}, \quad a = \frac{F \cdot n_f}{\pi p \cdot \rho_0^2} \times 10^6 \tag{3}$$

We get the equation of the outline cap derivative:

$$Z'(Y) = -\frac{Y^3}{\sqrt{a^2 Y^2 \cos^2\alpha - Y^6}} \tag{4}$$

where the following terms have been made dimensionless compared with ρ_0[1] (see Figure 4) such that the work can be independent from the minimum dimensions of shell radius.

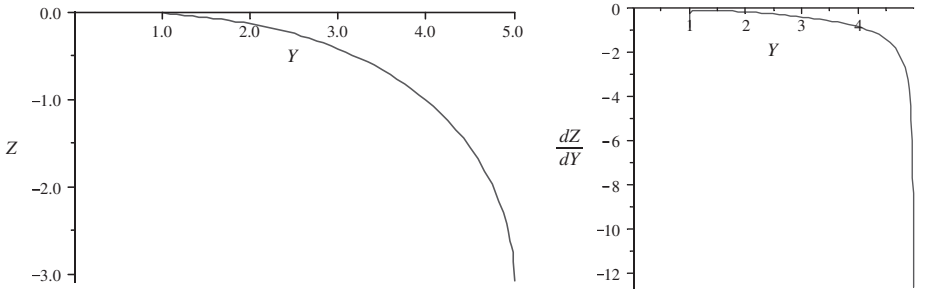

Figure 4. Example of cap meridian outline: (a) Z vs. Y (with $q = 1/25$); (b) Z' vs. Y (with $q = 1/25$).

The geodesic trajectories connect two arbitrary points on a continuous surface by means of the shortest possible way. Due to this characteristics property, geodesic paths lead to the most stable and economical technique for covering filament-wound structures.[16] In this work, such tow path kinds has been considered; this means that the math equation characterizing the tow path is the Cliraut [16] one:

$$\alpha(\rho) = \arcsin\left(\frac{\rho_0}{\rho}\right) \;\rightarrow\; \alpha(Y) = \arcsin\left(\frac{1}{Y}\right) \tag{5}$$

That replaced in (4) it makes:

$$Z'(p, Y) = -\frac{Y^3}{\sqrt{a^2(Y^2-1) - Y^6}} \tag{6}$$

that is defined in the interval:

$$Y \in \{Y_{\min}, Y_{eq}\} \;\Rightarrow\; \rho \in \{\rho_{\min}, \rho_{eq}\} \tag{7}$$

where the subscript *eq* and *min* are, respectively, stands for equator, and minimum allowable ρ for (6), and:

$$\rho_{\min}(q) = \sqrt{q} \cdot \rho_{eq}(q), \quad \rho_{eq}(q) = \frac{\rho_0}{\sqrt{q}}\sqrt{\frac{1-q^3}{1-q^2}} \quad \text{and} \quad q = \frac{\rho_{\min}^2}{\rho_{eq}^2} < 1 \tag{8}$$

From (6)–(8) the meridian outline (see Figure 4(a) and (b)) for $\rho \in \{\rho_{\min}, \rho_{eq}\}$ is:

$$Z(p, Y) = \int_{Y_{\min}}^{Y} Z'(\xi)d\xi \tag{9}$$

While the meridian outline for $\rho \in \{\rho_o, \rho_{\min}\}$is approximate with a straight path (we explain this later in this paper §2.2). The approximation about this zone is very low. With (8), can be easily estimated that $\rho_{\min}/\rho_0 > 1$, and for a typical values of $q \le 1/16$, $\rho_{\min}/\rho_0 < 1.025$ that is very close to 1.

2.2. Caps zone: mass and inner volume

Estimating the geometry of the meridian outline, and then the geometry of the cap, the mass of the cap has been evaluated that derives: (i) from the distribution of composite part thickness; (ii) from the liner quantity on the vessel internal surface (constant thickness); and (iii) from the polar boss mass.

Regarding the shell thickness, the tow angular variation (α, Figure 2) on the cap surface has been considered; the basic equation is:

$$\left(\rho + \frac{t}{2}\cos(\varepsilon)\right) \cdot 2\pi \cdot t = n_{he}\frac{s}{\cos(\alpha)} \quad \text{with} \quad \varepsilon(q, \rho) = \arctan\left(Z'|_{Y=\frac{\rho}{\rho_0}}\right) + \frac{\pi}{2} \tag{10}$$

where s is the cross-section area of a single tow; t is the shell thickness (function of the radius ρ) and ε is the angle of the normal to the meridian outline internal to the radial direction, as shown in Figure 6(a). Lastly n_{he} has been obtained by combining Equation (3) with the following equation:

$$a(q) = \left(\frac{\rho_{eq}}{\rho_0}\right)^2 \Big/ \sqrt{1 - \left(\frac{\rho_0}{\rho_{eq}}\right)^2} \tag{11}$$

This equation has been obtained from: (i) the axial balance characterized form the Equation (2); (ii) the geodetic conditions (Equation (5)); and (iii) the condition to the equator where $\beta = \pi/2$ (Figure 3).[16] After rewriting the (10) relatively to t and making it dimensionless compared to ρ_0 has been obtained:

$$t_{he}(p, q, \rho_0, \rho) = \frac{1}{\cos(\varepsilon)} \left[-\rho + \sqrt{\rho^2 + \frac{\cos(\varepsilon) \cdot n_{he} \cdot s}{\pi \cdot \cos(\alpha)}} \right] \tag{12}$$

The Equation (12) yields fair prediction for the shell thickness at a distance from the polar hole and fails to describe it in the close vicinity of the hole. Moreover, as tow approach the polar hole, angle α goes close to 90° and the shell thickness becomes infinitely high (Figures 5 and 6(b)).[14] For these reasons, the thickness in the interval $\rho = \{\rho_0, \rho^*\}$ con has been corrected with a constant thickness '$t_{he,\ \max}$', where ρ^* is equal to 5% of the interval $\Delta\rho = \rho_{eq} - \rho_0$ as it is shown in the work of Vasiliev [14]. The area refined by $\rho = \{\rho_0, \rho^*\}$ is crossed only by a portion of the whole tow number n_f and the winding type is almost circular (hoop winding).

The tow crossing number in the interval $\rho = \{\rho_0, \rho^*\}$ has been calculated through the following equation:

$$n^*_{he}(p, \rho_0) = \frac{n_{he} \cdot \Delta\varphi}{2\pi} \quad \text{for} \quad \rho = \{\rho_0, \rho^*\} \tag{13}$$

where $\Delta\varphi$ is the variation of the angular variable of the cylindrical coordinates defined in Figure 2 [17]:

$$\Delta\varphi = \int_1^{\rho^*/\rho_0} \frac{a}{\xi} \frac{1}{\sqrt{a^2(\xi^2 - 1) - \xi^6}} d\xi \tag{14}$$

The thickness has been considered constant and calculated as following (Figure 6(b)):

$$t_{he,\max}(p, \rho_0) = \frac{n^*_{he} \cdot s \cdot \rho_0}{\rho^* - \rho_0} \quad \text{for} \quad \rho = \{\rho_0, \rho^*\} \tag{15}$$

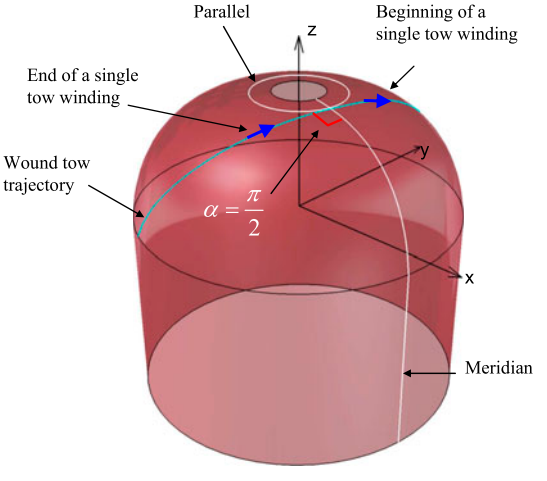

Figure 5. Example of tow winding on cap.

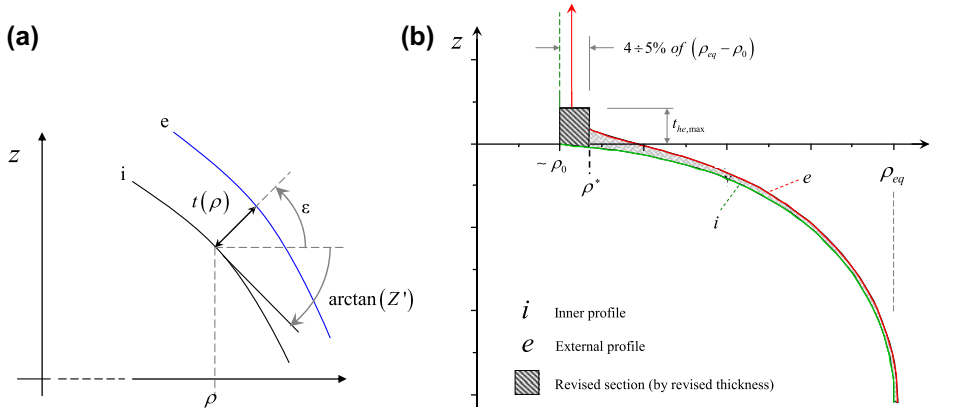

Figure 6. (a) Cap shell portion, with: t, shell thickness; i and e, internal and external meridian outline; (b) thickness correction close to polar hole.

In this way, the Equation (12) has been considered valid in the interval $\{\rho^*, \rho_{eq}\}$ while the (15) in the interval $\{\rho_0, \rho^*\}$. Known the meridian outline and the thickness distribution it was possible to evaluate the cap external outline as follow:

$$\begin{cases} \rho_{he,e}(p,q,\rho_0,\rho) = \rho + t \cdot \cos(\varepsilon) \\ z_{he,e}(p,q,\rho_0,\rho) = z(\rho) + t \cdot \sin(\varepsilon) \end{cases} \quad \text{with} \quad \begin{cases} t = t_{he,\max}(p,\rho_0) & \text{for} \quad \rho \in \{1,\rho^*\} \\ t = t_{he}(p,q,\rho_0,\rho) & \text{for} \quad \rho \in \{\rho^*,\rho_{eq}\} \end{cases} \tag{16}$$

In Figure 6(b), the surface included in the internal outline i and the external e represents the meridian section of composite shell. The volume of the caps area made of composite material has been calculated through the integral on domain Ω_{cap} delimited by external and internal surface of the cap (see Figure 7):

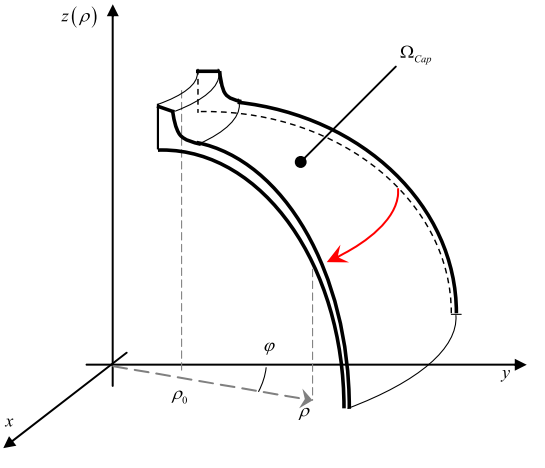

Figure 7. Meridian outline discretization of the cap.

$$v_{C,cap}(p,q,\rho_0) = \iiint_{\Omega_{cap}} dxdydz \quad v_{C,inner-cap}(p,q,\rho_0) = \iiint_{\Omega_{inner-cap}} dxdydz \tag{17}$$

Therefore, the relation allowing to evaluate shell mass (only helical winding) of the two caps is:

$$m_{C,cap}(p,q,\rho_0) = 2 \cdot v_{C,cap} \cdot d_C \tag{18}$$

Similarly has been proceeded for the definition of the equations related to: (i) liner volume in the cap, hypothesizing a constant thickness t_L and (ii) volume gas storage in caps $v_{inner\text{-}cap}$. Through the liner volume has been calculated its mass $m_{L,cap}$ multiplying it for the density of the material which it is made. The polar boss mass is (Figure 8):

$$m_{pb} = 2\pi \cdot A_{pb} \cdot \rho_{CG} \times 10^{-9} \cdot d_M = 2\pi \cdot Sm_z \times 10^{-9} \cdot d_M \tag{19}$$

where Sm_z and d_M are, respectively, the static moment of meridian section and the density of metallic material that makes the polar boss.

2.3. *Cylinder zone: mass and inner volume*

Similarly to the caps area, also for the cylindrical area mass is function of quantity of composite and liner that makes the vessel wall, and it is function: (i) of helical winding thickness (equal to helical stratification thickness at cap equator); (ii) of hoop winding thickness; (iii) of liner thickness (constant and equal to s_L); and (iv) of cylindrical zone height.

Composite quantity in the hoop direction is function of stress that such zone has to withstand; relation used is the following [17]:

$$F_\theta = F_{\theta,he} + F_{\theta,ho} = \sigma_{he} \cdot t_{he} + \sigma_{ho} \cdot t_{ho} = F_\theta \frac{\tan^2(\alpha_{eq})}{2} + \sigma_{ho} \cdot t_{ho}$$
$$\text{with} \quad \sigma_{ho}(p,q,\rho_0) = \frac{F_\theta}{t_{ho}}\left(1 - \frac{\tan^2(\alpha_{eq})}{2}\right) \tag{20}$$

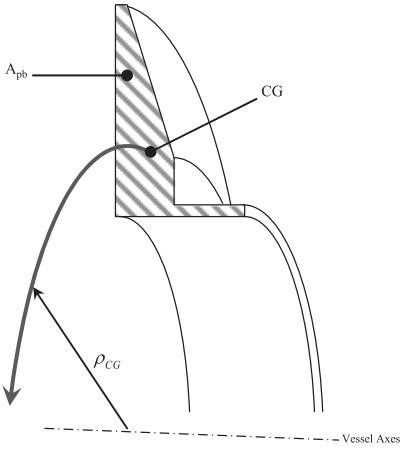

Figure 8. Description of Polar Boss, with: A_{pb}, cross-section area of polar boss; CG, cross-section center of gravity of polar boss; ρ_{CG}, radius of CG.

with:

$$\sigma_{ho} = \frac{n_{ho} \cdot F}{t_{ho}}, \quad F_\theta = p \cdot \rho_{eq} \times 10^{-6}, \tag{21}$$

where n_{ho} e t_{ho} are, respectively, layers number per length unit and hoop winding thickness; the subscript θ indicate the circumferential direction. Combining together the (20) and the (21) the equation of coils number has been obtained:

$$\begin{aligned} n_{ho}(p,q,\rho_0) &= n_f \left[\frac{\rho_{eq}}{\pi \cdot a \cdot \rho_0^2} \left(1 - \frac{\tan^2(\alpha_{eq})}{2} \right) \right] \quad \text{with} \quad \alpha_{eq} = \arcsin\left(\frac{\rho_0}{\rho_{eq}} \right), \\ a &= \frac{n_{he} F}{\pi \cdot p \cdot \rho_0^2} \times 10^6 \end{aligned} \tag{22}$$

Therefore, the hoop zone thickness is:

$$t_{ho} \cdot h = n_{ho} \cdot h \cdot at \Rightarrow t_{ho}(p,q,\rho_0) = n_{ho} \cdot at \tag{23}$$

For height h the fluid whole volume stored inside the vessel (v) has been considered, the relation obtained is the following:

$$h(p,q,\rho_0,v) = \frac{v - v_{inner-cap}}{\pi(\rho_{eq} - t_L)^2} \times 10^9 \tag{24}$$

Then through solids subtraction, the composite material volume of the shell and liner volume has been evaluated the (helical + hoop winding):

$$v_{C,cy}(p,q,\rho_0,v) = v_{C,ho} + v_{C,he} = \pi h \left[(\rho_{eq} + t_{ho} + t_{he})^2 - \rho_{eq}^2 \right] \tag{25}$$

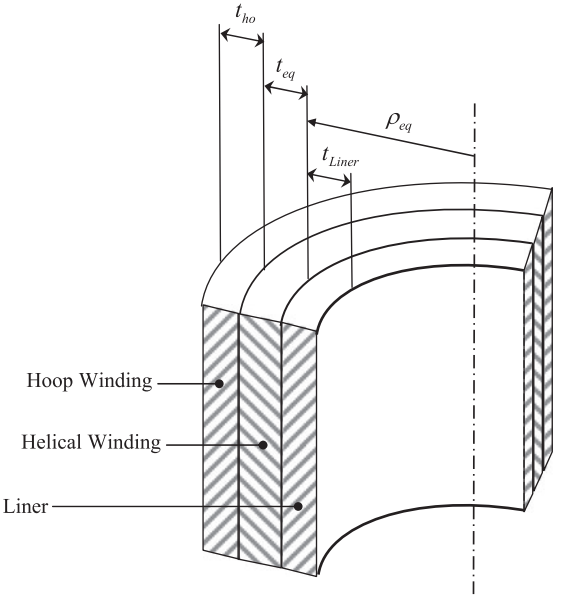

Figure 9. Description of cylinder zone wall.

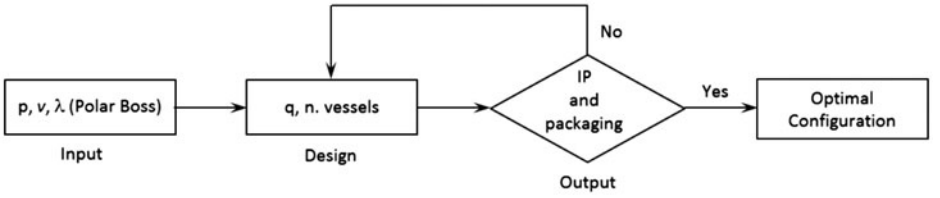

Figure 10. Flow chart for the definition of pressure vessels optimal configuration.

$$v_{L,cy}(p,q,\rho_0,v) = \pi h\left[\rho_{eq}^2 - \left(\rho_{eq} - t_L\right)^2\right] \tag{26}$$

After the shell and the liner mass has been possible to calculate (Figure 9):

$$\begin{aligned} m_{C,cy}(p,q,\rho_0,v) &= v_{C,cy} \cdot d_C \\ m_{L,cy}(p,q,\rho_0,v) &= v_{L,cy} \cdot d_L \end{aligned} \tag{27}$$

3. Performance index optimization

Equations listed in the previous paragraphs allow to calculate height, volume, mass, and in particular the 'performance index' of a configuration with one or more tanks in relation to the variables p, q, ρ_0 e v, according the logical flow reported in Figure 10.

The equation that defines the performance index is:

$$I_p(p,q,\rho_0,v) = \frac{v \cdot p}{m_{tot} g}, \quad \times \text{with} \quad m_{tot}\big|_{\substack{p=const \\ v=const}} = f(q,\rho_0) \tag{28}$$

considering the Equation (8) the diameter on equator is:

$$D_{eq} = 2 \cdot \rho_{\min} \cdot \sqrt{\frac{1}{q}} \tag{29}$$

and it is possible replacing q with D_{eq} in (28):

$$I_p(p,D_{eq},\rho_0,v) = \frac{v \cdot p}{m_{tot} g}, \quad \text{with} \quad m_{tot}\big|_{\substack{p=const \\ v=const}} = f(D_{eq},\rho_0) \tag{30}$$

Once the vessel pressure p has been defined, it is possible to optimize the 'performance index' minimizing $m_{tot} = m_{L,cy} + m_{C,cy} + 2 \cdot (m_{L,cap} + m_{C,cap} + m_{pb})$ and maximizing the storage gas volume v. To better understand the potential of analytical models below are some numerical examples; the parameters and the variables used are reported, respectively, in Tables 1 and 2.

In Figure 11, the I_p vs. v with D_{eq}-isocurve are shown, while in Figure 12 I_p vs. h_T with D_{eq}-isocurve and Vessel Number (NV) isocurve are shown. The 'Vessel Number' is the number of vessel necessary to storage 12.8 m^3 of gas, therefore the isocurve relative to Vessel Number equal to '4' is the isocurve of vessels with volume 12.8/4 m^3 = 3.2 m^3, and all equal between them. About this approach, there is a very interesting consideration between I_p and the system storage that was made by combining a defined vessel number. That is the performance index of a pressure vessel combination is the same of the single vessel included in the combination. The relations (29) and (30) give:

Table 1. Parameters used for the examples of Figures 12–16.

Parameters	Value	Parameters	Value
d_C (kg/m^3)	1600	t_L (mm)	1
d_L (kg/m^3)	960	F (N)	
d_M (kg/m^3)	2700	$\left(=\frac{s^+ \times at}{\gamma}=\frac{1500\times 0.7}{2.5}\right)$	420
Sm_z	1.5×10^{-6}	s^+, is the tensile strength γ, is the safety coefficient	
s (mm^2)	0.7	p (Pa)	3×10^6

Table 2. Variables used for the examples of Figures 11–17.

	Variables	Value
Figure 11	D_{eq} (mm)	400 ÷ 2800
(Equation (30))	Vessels Number (–)	1 ÷ 256
	(v (m^3))	(0.05 ÷ 12.8)
	ρ_0 (mm)	100
Figure 12	D_{eq} (mm)	400 ÷ 2800
(Equation (30))	v (m^3)	0.03 ÷ 10
	ρ_0 (mm)	100
Figures 13–17	q	1/25 and 1/100
(Equation (28))	v (m^3)	0.01 ÷ 10.42
	ρ_0 (mm)	10 ÷ 300

$$I_{p_{\mathrm{NV}}}=\frac{(v\cdot \mathrm{NV})\cdot p}{(m_{tot}\cdot \mathrm{NV})\cdot g}=\frac{v\cdot p}{m_{tot}\cdot g}=I_{p_{One}} \tag{31}$$

where NV, $I_{p_{\mathrm{NV}}}$ and $I_{p_{one}}$ are, respectively, the performance index of a combination of *more* vessels and the performance index of a single pressure vessel.

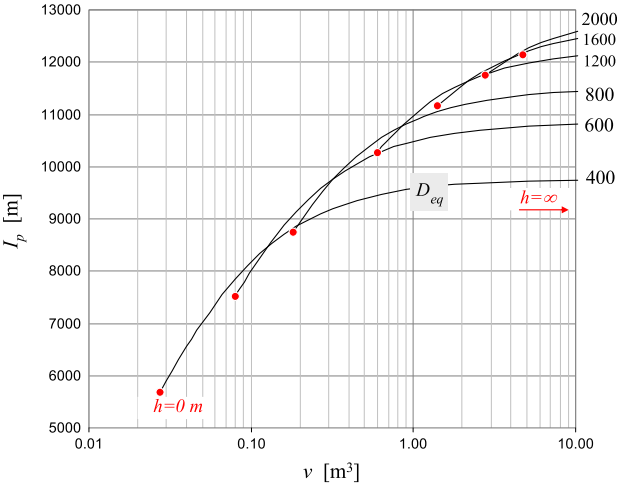

Figure 11. I_p vs. v with D_{eq}-isocurve (mm).

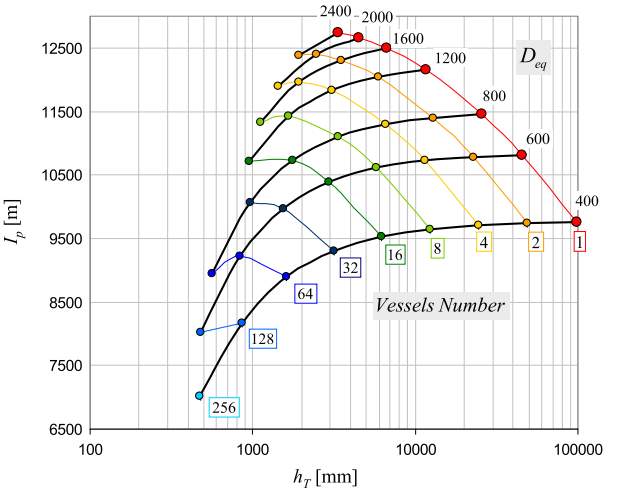

Figure 12. I_p vs. h_T with D_{eq}-isocurve (mm) and Vessel Number isocurve in order to storage 12.8 m^3.

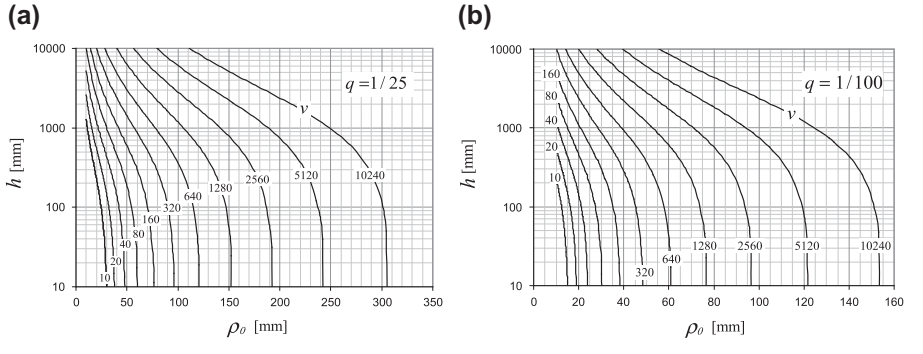

Figure 13. Cylinder Height (h (mm)) vs. ρ_0, (mm) with v-isocurve (10^{-3} m^3) for: (a) $q = 1/25$ and (b) $q = 1/100$.

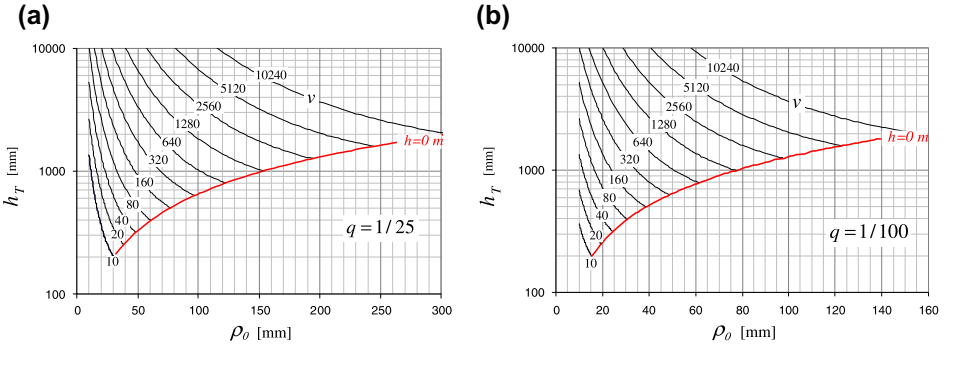

Figure 14. Total Height (TH (mm)) vs. ρ_0, (mm) with v-isocurve (10^{-3} m^3) for: (a) $q = 1/25$ and (b) $q = 1/100$.

Figures 13–17 show the example of some graphs related to interaction among I_p, m_{tot} and v, with $q = 1/25$ e $q = 1/100$.

As anticipated in the introduction, the aim of this work is to develop a method to optimize the performance index 'IP' for a dual purpose: (1) minimization of the weight, through the use of a single tank; (2) optimization of pressure vessels packaging considering the usable volume of the gas storage system (e.g. inside an aircraft aeronautical).

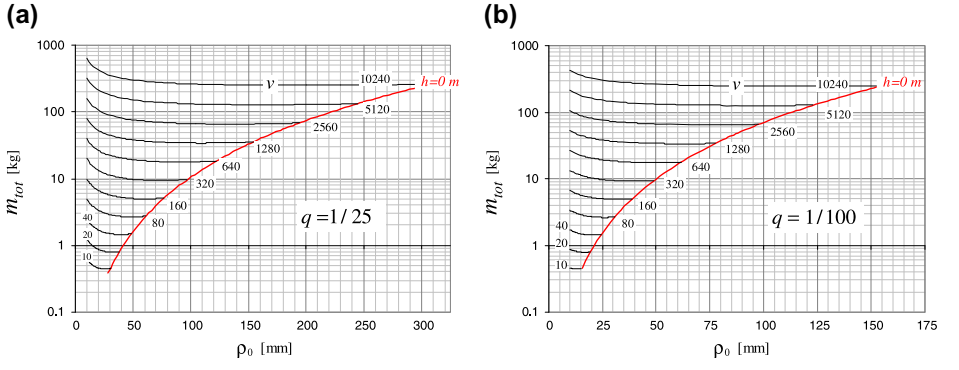

Figure 15. Mass vs. ρ_0 (mm), with v-isocurve (10^{-3} m^3) for: (a) $q = 1/25$ and (b) $q = 1/100$.

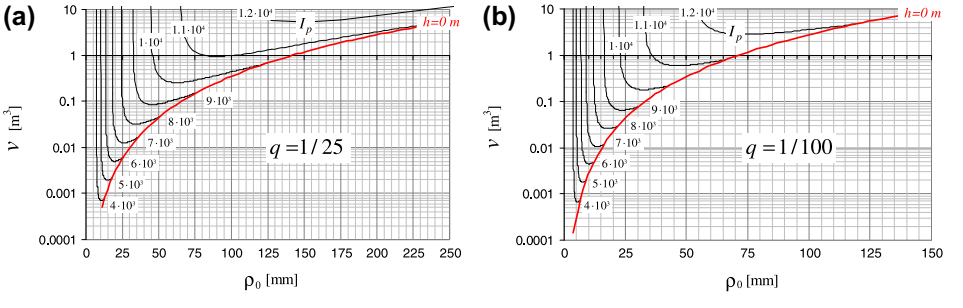

Figure 16. Volume vs. ρ_0, with I_p-isocurve for: (a) $q = 1/25$ and (b) $q = 1/100$.

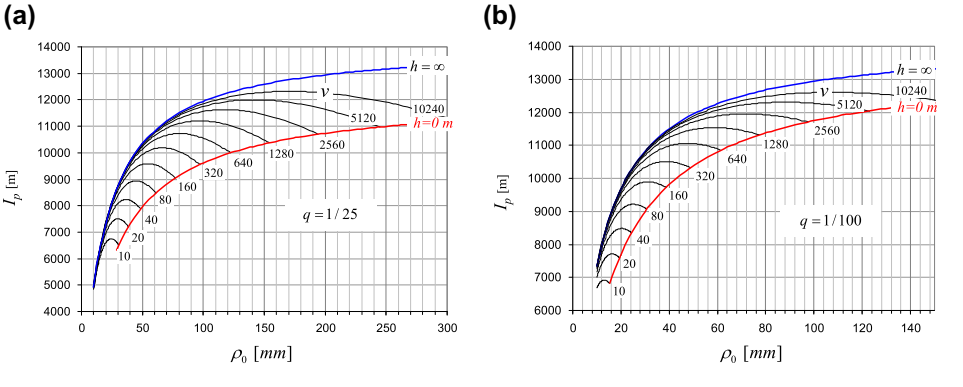

Figure 17. I_p vs. ρ_0 (mm), with v-isocurve (10^{-3} m^3) for: (a) $q = 1/25$ and (b) $q = 1/100$.

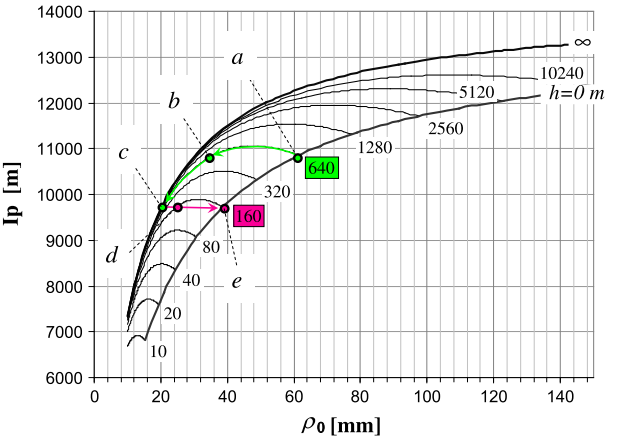

Figure 18. I_p vs. ρ_0 (mm), with v-isocurve (10^{-3} m^3) for $q = 1/100$.

The graphs shown in Figures 11–17 represent a flexible tool that makes the design/selection of the storage system (with one or more tanks) as a function of 'performance index' and of packaging necessity. In Figures 18 and 19, an example of design of the storage system for a fixed volume of 640×10^{-3} m^3 is shown; in particular, the trend of

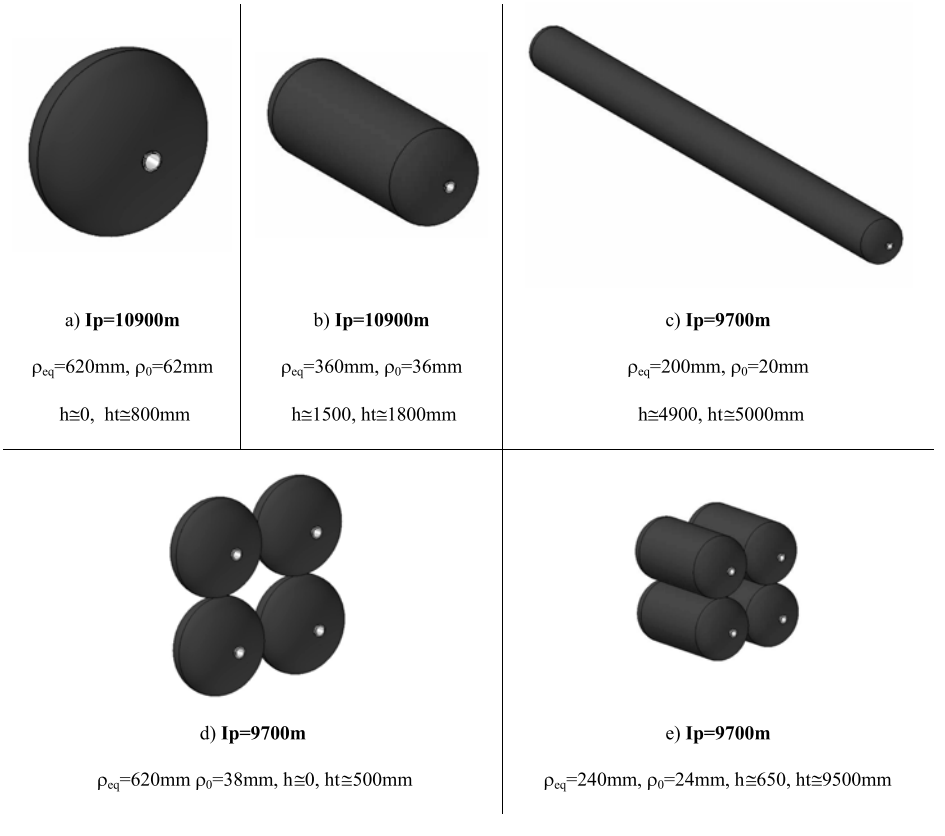

Figure 19. Example of volume gas storage with different geometric configuration.

IP as a function of variation of the geometric and number tanks. Of all possible combinations have been defined five points indicated 'a, b, c, d, e': the points 'a, b, c' are relative to configurations with a single vessel with constant volume ($640 \times 10^{-3}\,m^3$) and different geometry while the points 'd, e' relate to configurations with four vessels with a single volume equal to $(640 \times 10^{-3}/4) = 160 \times 10^{-3}\,m^3$. It may be noted further that 'a' and 'b' have the same IP but a different geometry; similar considerations can be extended to the all points that represent specific configurations.

4. Conclusions

This work aims to develop an analytics method allowing to optimize the 'index of performance' as a function of the structural/geometrical parameters and of the gas storage system/volume by the packaging of pressure vessels.

In particular, the performance index optimization 'IP' can be achieved by the use of a single tank, minimizing the weight, or by optimizing of the number/geometry of more pressure vessels considering the usable volume of the gas storage system (e.g. inside an aircraft aeronautical).

The examples in the paper show the high flexibility of the developed model that allows to achieve an optimum configuration as a function of the constraints imposed in terms of IP or packaging. In Figure 18, it is possible to evaluate the flexibility and potential of the model, in fact, defined a total volume of storage (equal to $640\,m^3$) it is possible to determine different solutions aimed at optimizing IP or the packaging: the points 'a, b, c' are related to configurations with a single tank with different geometries and values of IP while the points 'd, e' are related to four configurations with equal 'IP' but different geometries.

In conclusion, the use of this parametric method allow to optimize the index of performance as a function of one or more pressure vessels in order to optimize the needs/requirements of mass and/or packaging of the gas storage system.

Nomenclature

Original parameter	Normalized parameter	Description
I_p (mm)		Index of performance
d (kgm^{-3})		Density
p (Pa)		Vessel pressure
F (N)	a	Force that supports a single tow
ρ (mm)	Y	Shell radius
$\rho_{\min}$ (mm)	$Y_{\min} \sim 1$	Minimum shell radius
ρ_{PG} (mm)		Radius of polar boss gravity center
	q	$= Y_{\min}^2 / Y_{eq}^2$
$z(\rho)$ (mm)	$Z(Y)$	Meridian profile
	$Z'(Y)$	Meridian profile derivative
α (°)		Helical winding angle
β (°)		Angle between the axial direction and the tangent of inner cap meridian profile
φ (°)		Angle of cylindrical reference system
t (mm)		Shell thickness

m (kg)		Mass of pressure vessel
g (ms^{-1})		Gravity acceleration
v (m^3)	V	Storage gas volume
F_θ (Nm^{-1})		$= p \cdot \rho_{eq} \times 10^{-6}$
ρ_0 (mm)		Minimum radius of shell
	λ	Fraction of ρ_0 (opening of polar boss)
h (mm)		Height of cylinder area
n (–)	n^*_{he}	Number of tows
s (mm^2)		Tow section
A_{pb} (mm^2)		Cross-section area of polar boss
Sm_z (mm^2)		Static moment of meridian section (in respect to z axis)

Subscript			
he, *ho*	Helical, hoop winding	eq	Related to equator
C, L, M	Composite, liner, metal		

Acknowledgments

This work was carried out with the funding of the Italian MIUR (Ministry of University and Research). The authors are grateful to Lino Di Rubbo for supporting this work. Special thanks to Martina and Lorenzo S.

Note

1. Shell minimum diameter, close to polar boss.

References

[1] Burke KA. High energy density regenerative fuel cell systems for terrestrial applications. Ohio (OH): National Aeronautics and Space Administration; 1999. NASA/TM-1999-209429.
[2] Ko WL. Structural analysis of helios filament-wound tanks subjected to internal pressure and cooling. California (CA): National Aeronautics and Space Administration; 2005. NASA/TM-2005-212855.
[3] Simoes JAO, Wu ST, Loseries F. Visual simulation of the geodesic and non-geodesic trajectories of the filament winding. In: Graphics modelling and visualization in science and technology; 1993. p. 199–215.
[4] Lossie M, Brussel H. Design principles in filament winding. Compos. Manuf. 1994;5:5–13.
[5] Carvalho JD, Lossie M, Vandepitte D, Van Brussel H. Optimization of filament-wound parts based on non-geodesic winding. Compos. Manuf. 1995;6:79–84.
[6] Hojjati M, Safavi AV, Hoa SV. Design of domes for polymeric composite pressure vessels. Compos. Eng. 1995;5:51–59.
[7] Liang YD, Zou ZQ, Zhang ZF. Quasi-geodesics – a new class of simple and non-slip trajectories on revolutional surfaces. Proceedings of the 28th International SAMPE Technical Conference; 1996. p. 1071–1079.
[8] Park JS, Hong CS, Kim CG, Kim CU. Analysis of filament wound structures considering the change of winding angles through the thickness direction. Compos. Struct. 2002;55:63–71.
[9] Koussios S, Bergsma OK. Uninterrupted hoop and polar fibre paths on cylindrical pressure vessels using non-geodesic trajectories. Proceedings of the 17th Annual Conference of the American Society for Composites; West Lafayette; 2002.
[10] Koussios S, Bergsma OK, Mitchell G. Non-geodesic filament winding on generic shells of revolution. Proceedings of ICCM10; 2002 Jun; Brugge.

[11] Koussios S, Bergsma OK. Analysis of filament wound pressure vessels considering the laminate thickness variation through the meridional direction. Proceedings of the 14th International Conference on Composite Materials; 2002 Jul; San Diego, CA.
[12] Li SG, Cook J. An analysis of filament overwound toroidal pressure vessels and optimum design of such structures. J. Press. Vessel Technol. 2002;124:215–222.
[13] Evans JT, Gibson AG. Composite angle ply laminates and netting analysis. Proc. R. Soc. Lond. A. 2002;458:3079–3088.
[14] Vasiliev VV, Krikanov AA, Razin AF. New generation of filament-wound composite pressure vessels for commercial applications. Compos. Struct., Elsevier. 2003;62:449–459.
[15] ASME Boiler & Pressure Vessel Code, an international code, Section X. Fiber-reinforced plastic pressure vessels. ASME; 2004.
[16] Koussios S. Filament winding a unified approach [PhD thesis report]. Delft: Design & Production of Composite Structures, Faculty of Aerospace Engineering, Delft University Press; 2004.
[17] Kim CU, Kang JH, Hong CS, Kim CG. Optimal design of filament wound structures under internal pressure based on the semi-geodesic path algorithm. Compos. Struct. 2005;67: 443–452.
[18] Koussios S, Bergsma OK, Mitchell G. Non-geodesic filament winding on generic shells of revolution. J. Mater. Part L: Des. Appl. 2005;219:25–35.
[19] Koussios S, Bergsma OK. Friction experiments for filament winding applications. J. Thermoplast. Compos. 2006;19:5–34.
[20] Velosa JC, Nunes JP, Antunes PJ, Silva JF, Marques AT. Development of a new generation of filament wound composite pressure cylinders. 2009;69:348–1353.
[21] Wang R, Jiao W, Liu W, Yang F, He X. Slippage coefficient measurement for non-geodesic filament-winding process. Comp. Part A. Appl. Sci. Manuf. 2011;42:303–309.
[22] Sakata K, Ben G. Fabrication method and compressive properties of CFRP isogrid cylindrical shells. Adv. Compos. Mater. 2012;21:445–457.
[23] Tam WH, Ballinger Ian, Jaekle Don E. Conceptual design of space efficient tanks. In: 42nd AIAA Joint Propulsion Conference & Exhibit; 2006 Jul 9–12; Sacramento, CA.
[24] Koussios S, Beukers A. Influence of laminate thickness approximation methods on the performance of optimal filamentary pressure vessels. 23rd Annual Conference of the American Society for Composites; 2008 Sep; Memphis, TN, p. 9–11.
[25] Sorrentino L, Tersigni L. Filament-wound pressure vessels for high volume gas storage: an approaches to optimize the structural performance. ECCM14, 14th European Conference on Composite Materials; 2010 Jun 7–10; Budapest, Hungary. p. 522.
[26] Zu L, Koussios S, Beukers A. Design of filament-wound circular toroidal hydrogen storage vessels based on non-geodesic fiber trajectories. Int. J. Hydrogen Energy. 2010;35:660–670.